

AstroInspect: a web-based system to organize, assess, and visually inspect astronomical objects

NATANAEL M. CARDOSO ¹, CLAUDIA MENDES DE OLIVEIRA ², ANGELA C. KRABBE ²,
ANALÍA V. SMITH CASTELLI ^{3,4}, GUSTAVO B. OLIVEIRA SCHWARZ ¹, LILIANNE NAKAZONO ^{5,6},
RICARDO DEMARCO ⁷, MAIARA S. CARVALHO ², WILLIAM SCHOENELL ⁸, TIAGO RIBEIRO ⁹, ANTONIO KANAAN ¹⁰,
AND ANTONIO M. SARAIVA ^{1,11,12}

¹*Escola Politécnica, Universidade de São Paulo, São Paulo, 05508-010, SP, Brasil*

²*Instituto de Astronomia, Geofísica e Ciências Atmosféricas, Universidade de São Paulo, São Paulo, 05508-090, SP, Brasil*

³*Instituto de Astrofísica de La Plata, CONICET-UNLP, La Plata, B1900FWA, LP, Argentina.*

⁴*Facultad de Ciencias Astronómicas y Geofísicas, Universidad Nacional de La Plata, La Plata, B1900FWA, LP, Argentina*

⁵*Observatório Nacional, Rio de Janeiro, 20921-400, RJ, Brasil.*

⁶*Instituto de Física, Universidade de São Paulo, São Paulo, 05508-090, SP, Brasil*

⁷*Institute of Astrophysics, Facultad de Ciencias Exactas, Universidad Andrés Bello, Sede Concepción, Talcahuano, Chile*

⁸*The Observatories of the Carnegie Institution for Science, 813 Santa Barbara St, Pasadena, CA 91101, USA*

⁹*Rubin Observatory Project Office, Tucson, AZ 85719, USA*

¹⁰*Departamento de Física, Universidade Federal de Santa Catarina, Florianópolis, 88040-900, SC, Brasil*

¹¹*Center for Artificial Intelligence, Universidade de São Paulo, São Paulo, 05508-020, SP, Brasil*

¹²*Instituto de Estudos Avançados, Universidade de São Paulo, São Paulo, 05508-050, SP, Brasil*

ABSTRACT

The rapid growth of imaging and spectroscopic surveys has intensified the need for efficient tools that support visual inspection, a practice that remains essential for tasks such as classification, catalog refinement, and validation of automated methods. Existing solutions, however, often require the use of multiple platforms and complex workflows to integrate heterogeneous data. To address this challenge, we present the first release of the AstroInspect (<https://astroinspect.github.io>), a web-based system which ensures seamless access to several astronomical resources. The system provides an intuitive graphical user interface (GUI) through which users can upload catalogs of objects defined by celestial coordinates. AstroInspect automatically enriches these catalogs with complementary information, including imaging, spectroscopic, and photometric data retrieved in real time from surveys such as the Sloan Digital Sky Survey (SDSS), the Legacy Surveys (LS), and the Southern Photometric Local Universe Survey (S-PLUS). As an example of its scientific utility, we used AstroInspect to identify H α emission-line galaxies within a 7 deg radius in the direction of the Hydra I cluster (also known as Abell 1060) by visual inspection. Using a candidate set of 981 galaxies selected from S-PLUS photometric data, we produced a catalog of 80 galaxies with confirmed H α emission. These results highlight the potential of AstroInspect to support efficient visual inspection workflows.

Keywords: Astronomy software (1855) — Astronomy data visualization (1968) — Extragalactic astronomy (506) — Galaxies (573) — Emission line galaxies (459) — Galaxy clusters (584) — Abell clusters (9).

1. INTRODUCTION

Visual inspection of astronomical objects remains a fundamental step in observational astronomy, serving purposes such as morphological analysis (P. B. Nair & R. G. Abraham 2010; D. W. Darg et al. 2010; A. Baillard et al. 2011; J. S. Kartaltepe et al. 2015; S. Paudel et al.

2018; A. C. Krabbe et al. 2023; D. M. Alexander et al. 2023; D. Galdeano et al. 2025), sample cleaning (D. G. Lambas et al. 2012; A. V. Smith Castelli et al. 2024), and validation of automated methods (D. M. Alexander et al. 2023; L. Tan et al. 2025; C. R. Bom et al. 2021; N. M. Cardoso et al. 2021). This process leverages human sensitivity to visual patterns in images alongside an understanding of the underlying physical context, which remains challenging to fully encode in algorithms.

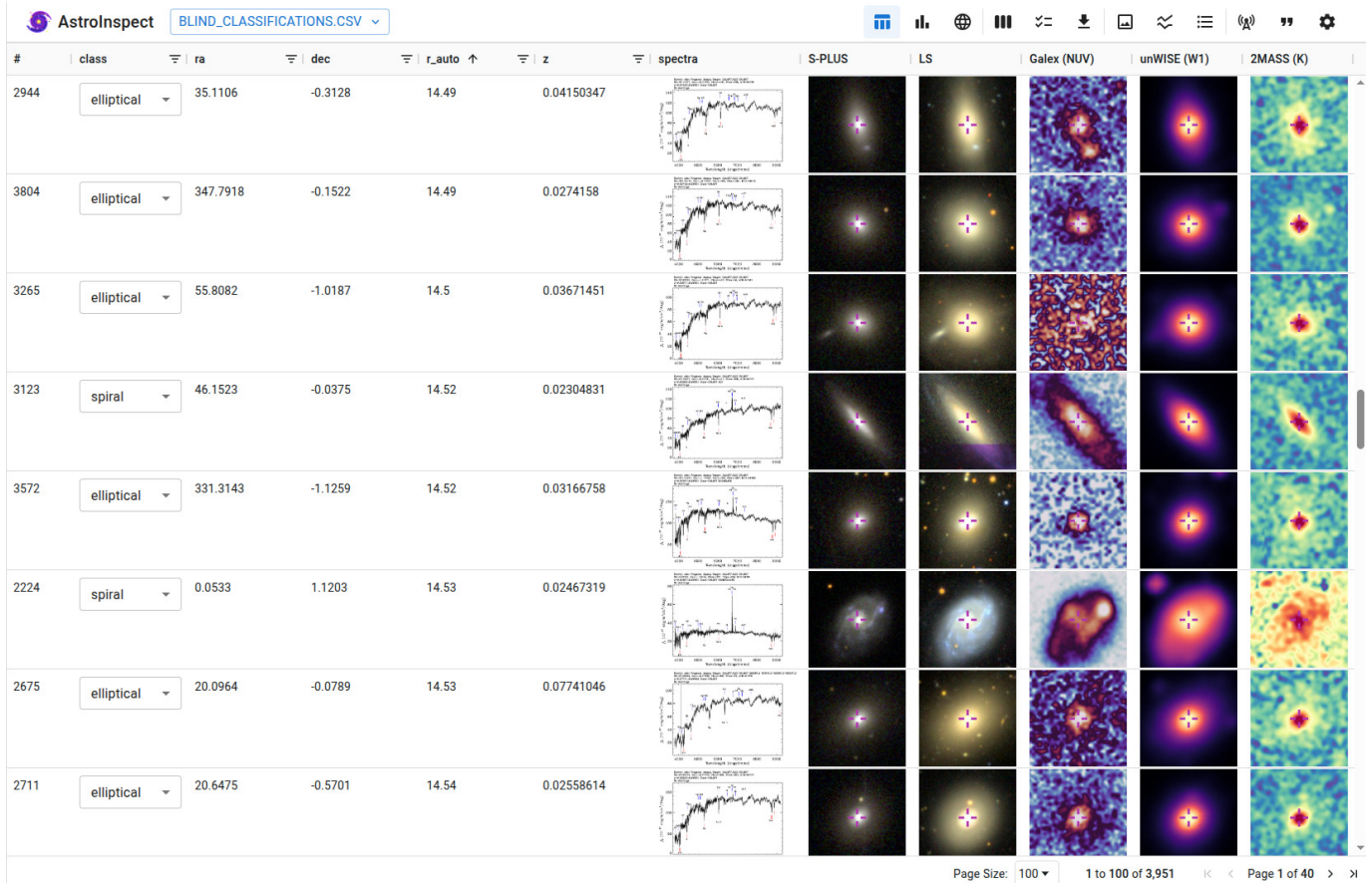


Figure 1. The AstroInspect interface streamlines visual inspection and scientific analysis by integrating spectroscopic, photometric, and imaging data into a single view, allowing “on-the-fly” comparative analyses. The user-uploaded catalog is organized into an interactive tabular interface that merges the input data (e.g. “ra”, “dec”, and “r_auto” columns) with dynamically-obtained data from remote services, such as redshift (e.g. “z” column from the SDSS spectroscopic catalog), the spectral energy distribution (“spectra” column), and color images from different surveys (e.g. “S-PLUS”, “LS”, “Galax (NUV)”, “unWISE (W1)”, and “2MASS (K)” columns, respectively). To support more effective visual assessment, AstroInspect also enables customization of image rendering parameters, including color stretch functions, colormap selection, and field-of-view adjustments.

Several tools have been developed for the access, analysis, and manipulation of astronomical data, addressing tasks such as the processing of tabular data, visualization of celestial images and atlases, spectral analysis, and the exploration of catalogs in remote databases.

For tabular data, the Starlink Tables Infrastructure Library Tool Set (STILTS; M. B. Taylor 2006) is a Java library for processing, cross-match, and statistical analysis of large catalogs, also accessible via a Command Line Interface (CLI). Its companion tool, the Tool for Operations on Catalogues and Tables (TOPCAT; M. Taylor 2017; M. B. Taylor 2005), provides a widely used Graphical User Interface (GUI) for interactive visualization and manipulation of tabular data.

For spectral analysis, Specview (I. Busko 2000, 2002) and the Virtual Observatory (VO) Spectral Analysis Tool (SPLAT-VO; P. W. Draper 2014; P. Škoda et al.

2014; P. Šaloun et al. 2016) offer GUI environments for the inspection and modeling of spectroscopic data.

In imaging, SAOImage DS9 (W. A. Joye & E. Mandel 2003) is a tool for visualizing astronomical images, supporting multidimensional data handling, region definition, and image overlays. Aladin (T. Boch et al. 2011; P. Paillou et al. 1994; F. Bonnarel et al. 2000) integrates sky surveys and catalogs, enabling visualization and exploration of sky atlases. Their web counterparts, SAOImage JS9 (T. Matilsky 2020) and Aladin Lite (M. Baumann et al. 2020), provide access to the core functionalities in web browsers.

In this work, we present the first release of the AstroInspect (<https://astroinspect.github.io>), a web-based system designed to address the gap related to softwares specialized in visual inspection and classification in the ecosystem of astronomical tools. The system integrates functionalities that enhances the efficiency of the work-

flow for morphological studies and exploratory analyses of astronomical catalogs by integrating data retrieval and visualization capabilities into a unified GUI (shown in Fig. 1). AstroInspect enables users to upload object defined by celestial coordinates, right ascension (RA) and declination (Dec). The application then automatically retrieves and displays associated imaging, spectroscopic, and photometric data. These data products may originate from both pre-configured major surveys and user-provided datasets, supporting various analytical workflows.

To illustrate its scientific application, we employed AstroInspect to identify galaxies with H α emission line in the direction of the Hydra I galaxy cluster (also known as Abell 1060, G. O. Abell et al. 1989). Candidate galaxies were first selected from S-PLUS photometric data and subsequently examined through visual inspection in AstroInspect. This analysis yielded a catalog of 80 galaxies with confirmed H α emission-line within an area with a projected radius of 7 deg, centered on the coordinates of Hydra I, providing a foundation for further studies and demonstrating the utility of the described tool.

In Section 2, we describe the data sources used by AstroInspect. In Section 3, we detail the system design and implementation. In Section 4, we summarize the system features. In Section 5, we present a scientific case study using AstroInspect to investigate H α emission candidates in the direction of Hydra I cluster. In Section 6, we discuss our findings. Finally, in Section 7, we present the conclusion and future work perspectives.

2. DATA SOURCES

The core feature of the AstroInspect is its ability to aggregate heterogeneous astronomical data within a unified graphical interface. This section summarizes the principal data sources integrated into the tool, outlining the distinct imaging, photometric, and spectroscopic products they provide.

2.1. The Large Sky Area Multi-Object Fiber Spectroscopic Telescope

The Large Sky Area Multi-Object Fiber Spectroscopic Telescope (LAMOST; X.-Q. Cui et al. 2012; G. Zhao et al. 2012), also known as the Guoshoujing Telescope, is a facility located at the Xinglong Station of the National Astronomical Observatories, China. Designed as a quasi-meridian reflecting Schmidt telescope with an effective aperture of 4 meters, LAMOST is optimized for wide-field spectroscopic observations and is equipped with 4,000 fibers on its focal plane. With over a decade of operation, LAMOST obtained spectra from more

than 25 million spectra, covering a footprint of $\sim 20,000$ deg² of the northern sky. These spectroscopic data is obtained through the LAMOST public API¹³.

2.2. The Dark Energy Spectroscopic Instrument

The Dark Energy Spectroscopic Instrument (DESI; DESI Collaboration et al. 2016) is a wide-field optical spectrograph with a focal plane equipped with 5,000 robotically controlled fiber positioners installed on the 4-meter Mayall Telescope at Kitt Peak National Observatory. The ongoing five-year survey will obtain spectra and redshifts for tens of millions of galaxies, stars, and quasars across approximately 14,000 deg² of the northern sky.

The DESI spectra is obtained through SPectra Analysis and Retrieable Catalog Lab (SPARCL; S. Juneau et al. 2024) API¹⁴ available at the NOIRLab Astro Data Lab science platform¹⁵ (M. Fitzpatrick et al. 2019; R. Nikutta et al. 2020).

2.3. The Sloan Digital Sky Survey

The Sloan Digital Sky Survey¹⁶ (SDSS; D. York et al. 2000) is an imaging and spectroscopic survey initiated the year 2000 employing a 2.5-meter telescope (J. E. Gunn et al. 2006) to map the northern sky across five bands, *u*, *g*, *r*, *i*, and *z* (M. Fukugita et al. 1996). The SDSS spectrograph (S. A. Smeed et al. 2013) obtained measurements of the Spectral Energy Distribution (SED) for more than 5 million objects of the northern sky.

Both photometric and spectroscopic data are obtained through the SkyServer¹⁷ (A. S. Szalay et al. 2002; M. Taghizadeh-Popp et al. 2020) Application Programming Interface (API).

2.4. The Southern Photometric Local Universe Survey

The Southern Photometric Local Universe Survey¹⁸ (S-PLUS; C. Mendes de Oliveira et al. 2019) is an imaging survey that covers a large portion of the southern sky using a wide-field telescope, the T80-South, located in Chile. It employs a 12-band photometric system that includes five broadband filters similar to those of the SDSS and seven narrow-band filters, selected to cover key spectral features. The narrow-band filters of S-PLUS are centered on the Balmer jump/[OII] (also

¹³ <https://lamost.org/openapi/docs>

¹⁴ <https://astrosparcl.datalab.noirlab.edu>

¹⁵ <https://datalab.noirlab.edu>

¹⁶ <https://sdss.org>

¹⁷ <https://skyserver.sdss.org>

¹⁸ <https://www.splus.iag.usp.br>

known as F378), Ca H + K (F395), H δ (F410), G band (F430), Mg b triplet (F515), H α (F660), and Ca triplet (F861) (see Table 2 in C. Mendes de Oliveira et al. 2019). The filters F395, F410, and F430 cover the H ϵ , H δ , and H γ lines, respectively. This wide spectral coverage, ranging from ultraviolet to near-infrared, enables the construction of photometric SEDs (also called photo-spectra), which are particularly valuable when spectroscopic SEDs (also called spectra) are unavailable.

The imaging data, reduced by the Multiband Astronomical Reduction (MAR) package (G. O. Schwarz et al. 2025), and photometric catalog from S-PLUS are retrieved from the S-PLUS Cloud API¹⁹.

2.5. DESI Legacy Imaging Surveys

The DESI Legacy Imaging Surveys²⁰ (LS; A. Dey et al. 2019) are a collaborative effort comprising three public projects: the Dark Energy Camera (DECam) Legacy Survey (DECaLS; R. D. Blum et al. 2016), the Beijing-Arizona Sky Survey (BASS; H. Zou et al. 2017), and the Mayall z -band Legacy Survey (MzLS; D. R. Silva et al. 2016). Together, these surveys cover both the northern and southern hemispheres, capturing images of the extragalactic sky in four optical bands (g , r , i , and z) using telescopes at the Kitt Peak National Observatory and Cerro Tololo Inter-American Observatory.

The imaging data is retrieved from the Legacy Survey Sky Browser API²¹ and the photometric catalog is obtained through the NOIRLab Astro Data Lab science platform.

2.6. Hierarchical Progressive Surveys

In addition with the previously mentioned data sources, AstroInspect also integrates imaging information from several Hierarchical Progressive Surveys (HiPS; P. Fernique et al. 2015) covering a wide spectral range. The available surveys are the Galaxy Evolution Explorer (Galex; D. C. Martin et al. 2005), the SDSS, the Skymapper (C. A. Onken et al. 2024), the Panoramic Survey Telescope and Rapid Response System (Pan-STARRS; K. C. Chambers et al. 2016), the Dark Energy Survey (DES; Dark Energy Survey Collaboration et al. 2016), the Hyper Suprime-Cam Subaru Strategic Program (HSC; H. Aihara et al. 2018), the Deep Near-Infrared Southern Sky Survey (DENIS; N. Epchtein et al. 1997), the Two Micron All Sky Survey (2MASS; M. F. Skrutskie et al. 2006), the United King-

dom Infrared Telescope (UKIRT; S. J. Warren et al. 2007) Infrared Deep Sky Survey (UKIDSS; A. Lawrence et al. 2007), the UKIRT Hemisphere Survey (UHS; S. Dye et al. 2018), the Unblurred Wide-field Infrared Survey Explorer (unWISE; E. L. Wright et al. 2010; D. Lang 2014), and the Karl G. Jansky Very Large Array Sky Survey (VLASS; M. Lacy et al. 2020). For redundancy purposes, AstroInspect also includes HiPS for the LS.

The imaging data is retrieved from Hips2Fits²² service provided by the Centre de Données Astronomiques de Strasbourg²³ (CDS).

3. SYSTEM DESIGN AND IMPLEMENTATION

3.1. System overview and design concept

Visual classification studies that involve inspecting large astronomical catalogs frequently begin with the development of dedicated graphical tools to support the classification process (e.g., P. B. Nair & R. G. Abraham 2010; A. Baillard et al. 2011; J. S. Kartaltepe et al. 2015; M. M. Boyce et al. 2023). To support future research with a flexible and reusable solution, we have developed AstroInspect with the following key features:

1. **System generality and extensibility:** the system shall support multiple scientific workflows and shall allow the integration of both externally published survey data and user-provided local datasets.
2. **Automated data acquisition:** the system shall provide configurable mechanisms for the automatic retrieval of data from multiple external services.
3. **Performance and concurrency:** the system shall employ concurrent data-access strategies to reduce latency and maintain responsiveness when processing large catalogs.
4. **Multi-survey data integration:** the system shall combine data products from multiple astronomical surveys to maximize spatial and spectral coverage for each object.
5. **Multi-modal data visualization:** the system shall present imaging and spectroscopic data concurrently to support accurate visual inspection and classification tasks.

¹⁹ <https://splus.cloud>

²⁰ <https://legacysurvey.org>

²¹ <https://legacysurvey.org/viewer>

²² <https://alasky.cds.unistra.fr/hips-image-services/hips2fits>

²³ <https://cds.unistra.fr>

6. **Object classification and annotation:** the system shall provide functionality for users to assign classifications and annotations to astronomical objects directly within the input table and shall store these results for subsequent analysis or export.
7. **Usability and accessibility:** the system shall provide an intuitive user interface that does not require programming expertise, virtual environment configuration, or software installation.

Based on these functional requirements, we designed AstroInspect to provide an integrated environment for the inspection, visualization, and classification of astronomical catalogs through a streamlined and accessible workflow, as shown in Fig. 1. The user initiates the process by loading an input table, which can be stored locally or accessed remotely. For each row (representing a single astronomical object), the application automatically queries remote services based on the object’s coordinates (RA, Dec). The retrieved material augments the input catalog with imaging, spectroscopic, or catalog data products, depending on the user’s configuration. To ensure broad applicability, the tool also supports the display of arbitrary local or remote datasets supplied by the user.

Furthermore, the system includes native annotation functionality, enabling users to record classifications or comments directly within the interface. The architecture that enables this workflow comprises several interconnected components, described in Section 3.2.

3.2. System components

This section provides a high-level description of the system’s core components, which are responsible for orchestrating data retrieval, state management, and user interaction. The overall architecture diagram is shown in Fig. 2.

3.2.1. Table State Manager

The Table State Manager (TSM) maintains the application’s global state throughout execution, providing a centralized interface for accessing and modifying system data. It stores the user-loaded table, retrieved survey products, and all user interactions, including configuration choices and annotations. All system components interact with the TSM to read or update the current state, ensuring consistent data flow and coordinated behavior across the application.

3.2.2. Table I/O Handler

The Table Input/Output (I/O) Handler (TIOH) manages the import and export of tabular data and ex-

tracts essential metadata, such as the names of coordinate columns. During data loading, the TIOH parses the input table and dispatches the extracted content in internal representation to the TSM for storage. When exporting, it retrieves the current table state from the TSM (including user-driven modifications such as filtering, reordering, or sorting) and generates a downloadable file for the user.

3.2.3. Tasks

Tasks refer to all operations that retrieve remote resources or process acquired data for display in the GUI. Tasks are classified as either compute-bound or I/O-bound.

Compute-bound tasks require local processing prior to visualization (e.g., generating photometric SEDs from S-PLUS magnitudes). These tasks are handled by the Worker component (Fig. 2), which executes Python code in isolated threads via the browser’s Web Worker API²⁴. This prevents computationally intensive operations from blocking the responsiveness of the GUI. Each Worker contains three internal modules: the Python Bootstrapper, which initializes the interpreter and the required packages; the Python Runtime, which executes python code related to HTTP-based data retrieval and processing; and the Request Listener, which manages communication between the Python interpreter via Foreign Function Interface (FFI) and the main thread via Inter-Thread Communication (ITC).

Conversely, I/O-bound tasks primarily involve data transfer with minimal processing (e.g., displaying pre-cut images obtained from remote services). These tasks execute on the main thread using non-blocking JavaScript functions managed by the browser event loop.

This design separates computational and I/O workloads to optimize performance. Workers enable parallel execution of compute-intensive tasks but incur overhead from thread initialization, Python runtime startup, transformation of the memory representation of objects between Python and Javascript runtimes (called marshaling), and transport across ITC boundaries. Asynchronous functions avoid these costs by sharing the memory space with the main application thread, but they are unsuitable for long computation tasks.

3.2.4. Task Pools

The task pools limits the number of concurrent operations executed for each data provider. AstroInspect implements two task pools: the Worker Task Pool (WTP)

²⁴ <https://html.spec.whatwg.org/multipage/workers.html>

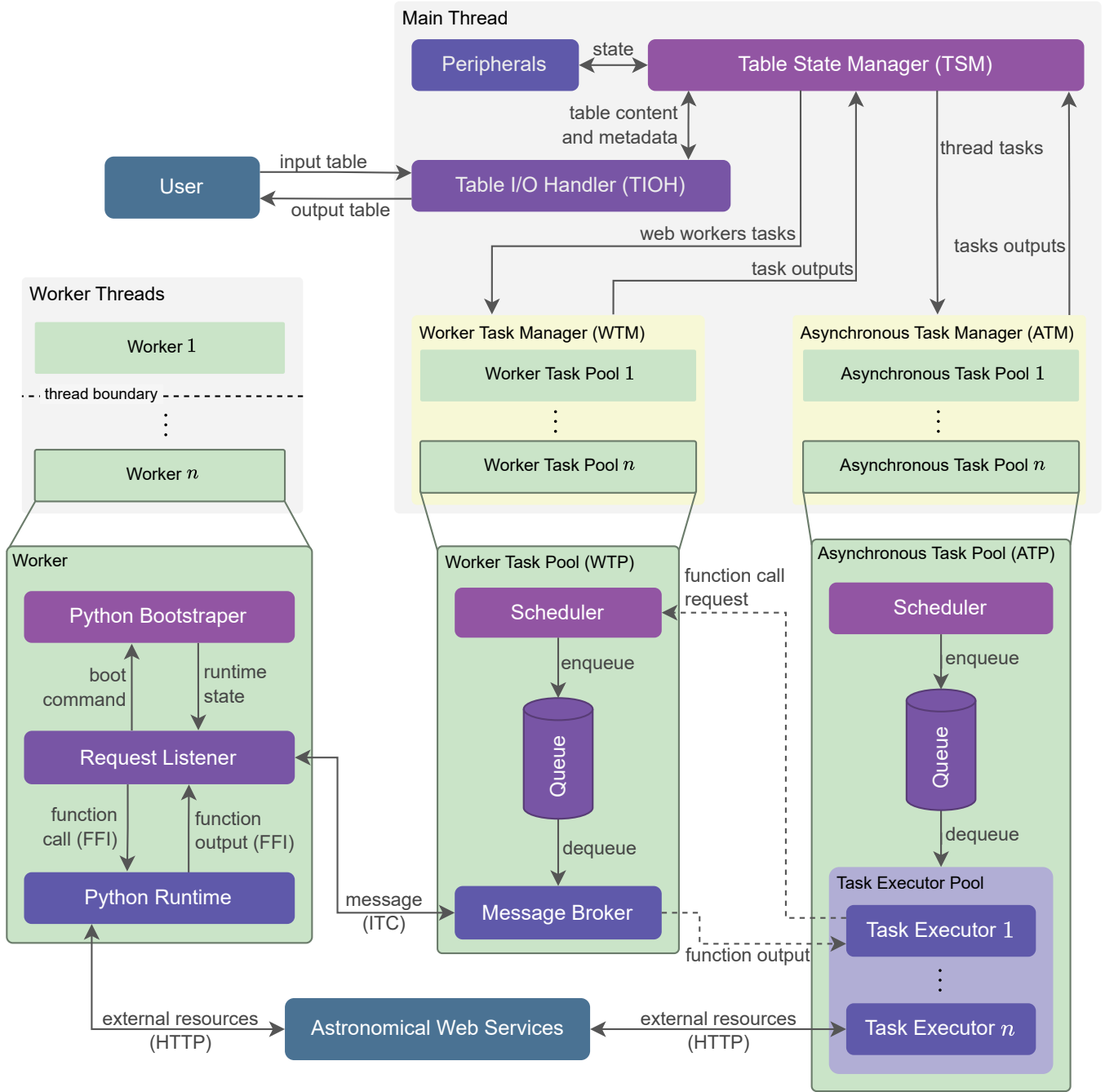


Figure 2. A schematic of the AstroInspect system architecture, illustrating the interaction of its core components. The Table State Manager (TSM) maintains the global application state, and the Table I/O Handler (TIOH) manages data import and export. Concurrent task execution is managed by two specialized pools: the Worker Task Pool (WTP), which orchestrates computationally intensive tasks in isolated threads via workers running Python code, and the Asynchronous Task Pool (ATP), which handles I/O tasks via non-blocking Javascript functions running in main thread. The Request Listener of the Worker interacts with the Python Runtime calling functions and receiving their results back via Foreign Function Interface (FFI), which enables data exchange between the JavaScript and Python. The Message Broker facilitates Inter-Thread Communication (ITC) between workers and the main thread. The executors (workers or asynchronous functions) can retrieve resources from Astronomical Web Services through Hypertext Transfer Protocol (HTTP). After a task is completed, its results (output data or error message) are dispatched to the TSM, being able to be displayed in the GUI. Peripheral components interact with the TSM based on user actions. Solid arrows represent the data flow between components, while dashed arrows shows an optional relation between ATP and WTP forming hybrid tasks, in which the ATP initiates the task by performing I/O operations, forwards processing workloads to the WTP, and receives the result back, following a client-server relationship.

for compute-bound tasks and the Asynchronous Task Pool (ATP) for I/O-bound tasks. This separation provides fine-grained control over concurrency, reduces load on external services, and prevents processing bottlenecks. It also enables hybrid execution workflows, in which tasks begin in the ATP for remote data acquisition and continue in the WTP for local processing, as indicated by the dashed arrows in Fig. 2.

Both task pools follow a producer–consumer model (E. W. Dijkstra 1968, 1972). The Scheduler component acts as the producer, generating and queuing task messages that specify the function to be executed, its arguments, and the preassigned executor within the pool. Task assignment follows a round-robin scheduling strategy.

In the WTP, workers are managed through a pre-allocated pool to avoid the overhead of dynamic thread creation. The Message Broker acts as the consumer, dequeuing tasks and dispatching them to the worker selected by the Scheduler via Inter-Thread Communication (ITC). Upon creation, each worker’s Request Listener automatically subscribes to the Message Broker, allowing it to receive function-call requests and return execution results through the communication same channel.

In contrast, the ATP uses a Task Executor Pool as the consumer. It executes asynchronous, non-blocking functions on the main thread controlled by browser’s event loop.

3.2.5. Task Managers

The system employs high-level task manager components to orchestrate concurrency. AstroInspect implements two managers: the Worker Task Manager (WTM) for thread-based pools (WTPs) and the Asynchronous Task Manager (ATM) for non-blocking function pools (ATPs). Each manager is responsible to create, control, and terminate dedicated task pool instances responsible for all data retrieval and processing tasks from a specific web service, such as SkyServer, S-PLUS Cloud, or Astro Data Lab.

3.2.6. Peripherals

The peripheral components include all system modules not directly involved in concurrent task orchestration and therefore not shown in Fig. 2. These elements, such as configuration forms and interface utilities, interact with the TSM to read the current application state and dispatch updates when user actions or settings require changes. Their role is to support user interaction while maintaining consistency across the interface.

3.3. Implementation details

We adopt a reactive programming paradigm to coordinate data flow among system components under high data-throughput conditions. In this model, the interface updates automatically in response to changes in the application state (managed by the TSM, see Fig. 2), such as the completion of remote data requests or user interactions. This approach ensures that data products appear in the GUI as soon as they become available, minimizing the latency in the visual feedback and improving the user experience.

To support this architecture, the client interface is developed using Next.js²⁵, a framework built on React.js²⁶ that supports reactive programming and static site generation. By serving the application as precompiled static assets, the system avoids server-side page rendering at runtime, reducing the backend complexity.

WebAssembly (WASM) is a portable binary format that enables high-performance execution of code from languages other than Javascript directly within the web browser. For this work, we leverage Pyodide, a distribution of the scientific Python ecosystem compiled to WASM. This provides client-side access to essential astronomical Python libraries without local installation, a capability increasingly adopted for scientific web ap-

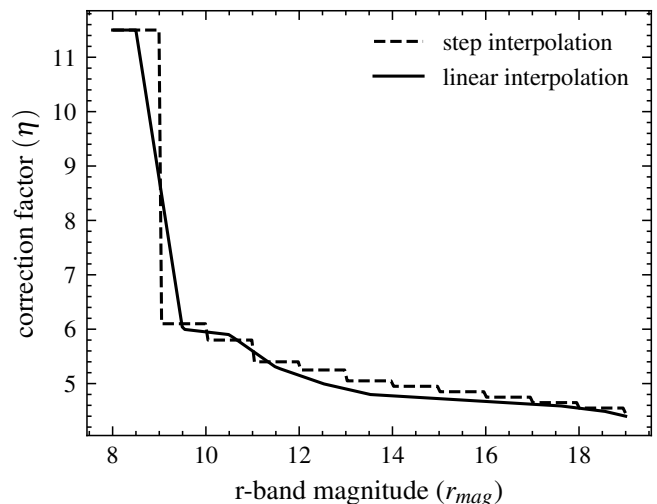


Figure 3. Empirical correction factor (η) as a function of the r -band magnitude (r_{mag}) used to estimate the optimal field of view (FOV) for the stamps. Two interpolation schemes were employed to represent η : step interpolation (rank 0, dashed line) and linear interpolation (rank 1, solid line). The linear interpolation was implemented in AstroInspect, as it provides a better fit for brighter objects.

²⁵ <https://nextjs.org>

²⁶ <https://react.dev>

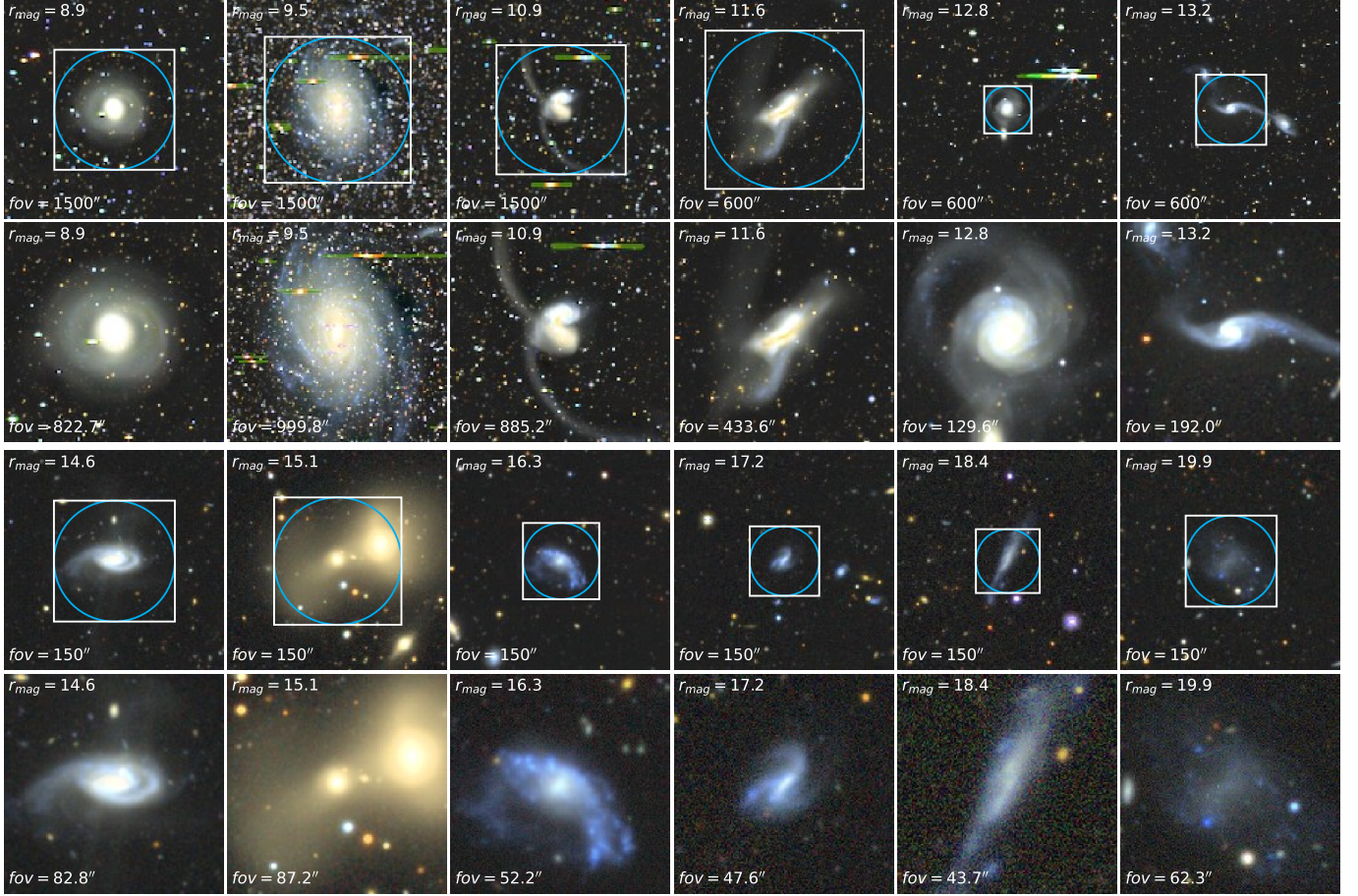


Figure 4. Adjustment of the LS image cutouts for twelve galaxies. The upper two rows show objects with r -band magnitude range from 8 to 14 mag, while the lower two rows show objects with r -band magnitude range from 14 to 20 mag. In the first and third rows, the panels illustrate the initial fields of view (FOVs) manually defined prior to the visual inspection procedure described in Section 3.4. The blue circle marks the effective radius (r_e), scaled according to the Eq. 1. The white square indicates the bounding box associated with this circle. The second and fourth rows present the final automatically adjusted cutouts, whose FOVs correspond to the bounding boxes shown above.

plications (e.g., M. Torrens-Fontanals et al. 2024; K. D. Harris & G. Greenbaum 2024; D. Ji et al. 2024; S. Heil et al. 2025; R. Peeters et al. 2025; K. Žáková & C. Beňačka 2025). This choice directly fulfills the accessibility requirement central to our system design (Section 3.1), delivering an analysis environment that operates entirely within a web browser.

Python code is used to generate both photometric and spectroscopic SED plots from S-PLUS and DESI surveys, respectively, using the Matplotlib package (J. D. Hunter 2007), and to handle table I/O operations with Astropy package (The Astropy Collaboration et al. 2013, 2018, 2022).

3.4. Image cutout preparation

A key consideration when creating image cutouts is the angular field of view (FOV), which defines the extent of the sky covered. When dealing with heterogeneous datasets that include objects with a wide distribution

of sizes and distances, a single fixed FOV for the entire dataset can complicate the inspection process. Smaller objects will be displayed in a very reduced form or, conversely, large objects will be presented in very enlarged sections, making it impossible to see their entire structure. Therefore, an automatically adjusted FOV ensures that each object can be visualized within its context and in relation to its morphological characteristics.

The effective radius (r_e) was adopted as the basis for estimating the FOV of each object. This parameter, defined as the radius enclosing half of the total emitted light, is provided in the LS photometric catalog (Section 2.5). To approximate the FOV, r_e must be scaled by a correction factor (η), which depends on the object's brightness, expressed by its r -band magnitude (r_{mag}), as given in Eq. 1:

$$\text{fov}(r_{\text{mag}}, r_e) = 2\eta(r_{\text{mag}})r_e \quad (1)$$

The correction factor (η) was empirically derived through the visual inspection of 12 galaxy samples, each comprising 500 objects within intervals of 1 mag in the r band, covering the brightness range from 8 to 20 mag. To perform this inspection, we employed AstroInspect’s functionality for loading custom images (Section 4.5), which enabled the assessment of each sample and the determination of optimal correction factor values. Both step interpolation (spline of rank 0) and linear interpolation (spline of rank 1) were evaluated, and the resulting dependence of η on r_{mag} is presented in Fig. 3. We choose to use the linear interpolation in the AstroInspect implementation, as it fits better on brighter objects.

To illustrate the developed approach, Fig. 4 presents the automatic fitting results for a randomly selected galaxy from each of the 12 samples, corresponding to the magnitude intervals 8-20 mag.

AstroInspect retrieves adjusted image cutouts in three steps. First, the photometric data (r_e and r_{mag}) of the object are retrieved by the VO service provided by Astro Data Lab using the Simple Cone Search (SCS; R. Plante et al. 2008) protocol, parametrized with the RA and Dec coordinates of the object from the input table and a search radius of 1.5 arcsec. Then, the FOV is calculated using Eq. (1) with the retrieved r_e and r_{mag} . Finally, a request is made to the image services to retrieve an image cutout within the calculated FOV.

4. SYSTEM FEATURES

In this section, we highlight the signature features available in AstroInspect.

4.1. SDSS catalogs access

Cross-referencing observational data across multiple catalogs is often essential in astronomical research to fully characterize observed objects. AstroInspect enables real-time retrieval of columns from SDSS photometric and spectroscopic catalogs via the SkyServer API, allowing the display of measurements such as magnitudes, redshifts, and other parameters directly selected through the GUI.

4.2. Image cutout visualization

The image cutout viewing feature in AstroInspect enables the visual inspection of astronomical objects. Once a table is loaded, AstroInspect automatically downloads and displays image cutouts for each object from the selected sources. Images can be retrieved from several surveys (detailed in Sec. 2) and displayed simultaneously to facilitate comparative analyses, since the surveys can differ in characteristics, such as spatial or spectral coverage, number of filters, and observational depth.

AstroInspect can also display both local and remote images from user-defined sources. To enable this functionality, the user specifies a table column containing a resource identifier (RI) that uniquely defines the image location for each table row. Optional prefix and suffix strings may also be provided. AstroInspect constructs the image address for each object by concatenating the prefix, RI, and suffix in sequence. Any image format supported by modern web browsers can be loaded (e.g., JPG, PNG, GIF, WEBP).

For example, if the user specifies a RI column which contains values such as J012502.90+002640.2, and the user sets the prefix to `https://example.com/i/` and the suffix to `.jpg`, AstroInspect generates URLs of the form `https://example.com/i/J012502.90+002640.2.jpg` for each object. The same mechanism applies to local images, where the prefix corresponds to a directory path and the suffix specifies the file extension.

4.3. Spectral energy distribution visualization

Spectroscopic SEDs are retrieved from SDSS, DESI, or LAMOST. For the many objects lacking spectroscopy, photometric SEDs provide a crucial alternative. AstroInspect leverages the broad spectral coverage of S-PLUS, with its 12-band filter system, to generate these photometric SEDs in real time.

4.4. Exploratory data analysis tool

The statistical visualization tools included in AstroInspect are scatter plots, histograms, and color-color diagrams. These graphs can be used to refine data samples by removing unreliable objects for visual inspection. Additionally, AstroInspect integrates the Aladin-Lite (M. Baumann et al. 2020) package within the interface, thus enabling users to visualize the spatial arrangement of objects in the sky, overlay additional datasets, and interact with sky atlases.

4.5. Interaction with other Virtual Observatory applications

AstroInspect supports communication with other VO-compliant tools via Simple Application Messaging Protocol (SAMP; M. B. Taylor et al. 2015; T. Boch et al. 2012). SAMP enables real-time messaging between applications, allowing seamless data exchange without manual file handling. Through this protocol, AstroInspect can load tables from other graphical applications (e.g., Aladin or TOPCAT), or programmatically using packages such as Astropy, which provides Python-based interface to SAMP messaging.

4.6. Object classification

The classification tool in AstroInspect allows users to define custom categories and assign them to objects within the catalog, with the results exportable as a table. This functionality supports a broad range of scientific applications, such as morphological classification, catalog cleaning, and targeted sample selection. For example, Fig. 1 illustrates a use case in which the “class” column includes the user-defined labels “elliptical” and “spiral.” To improve efficiency during large catalog inspections, users may also assign keyboard shortcuts to each class, reducing repetitive interactions.

5. SCIENCE CASE STUDY: EMISSION-LINE GALAXIES IN THE DIRECTION OF THE HYDRA I CLUSTER

Galaxy clusters are among the most massive gravitationally bound structures in the universe, comprising hundreds to thousands of galaxies embedded within a hot, diffuse intracluster medium. Interactions between cluster galaxies and the intracluster medium – including mechanisms such as ram-pressure stripping, strangulation, and tidal forces – play a critical role in driving morphological transformations and quenching star formation in member galaxies (J. E. Gunn & J. R. Gott 1972; J. S. Gallagher & J. P. Ostriker 1972; B. Moore et al. 1996; Y. L. Jaffé et al. 2015). In this context, visual inspection of galaxies in clusters remains a valuable approach for identifying and characterizing the wide range of morphological changes induced by environmental effects.

In this science example, we show the use of AstroInspect to build a catalog of galaxies with H α emission in the direction of the Hydra I cluster (also known as Abell 1060; G. O. Abell et al. 1989) by visual inspection. Hydra I is of particular interest for this study, as its proximity enables the H α emission of disk galaxies in the cluster to be detected by the F660 filter and thus be very well highlighted in the 12-band RGB images from the S-PLUS survey, as shown in previous studies (C. Lima-Dias et al. 2020, 2023).

We adopt $\alpha, \delta = 10:36:41.8, -27:31:28$ (J2000) as central position of Hydra I (E. K. Panagoulia et al. 2014), a heliocentric redshift $z_{\text{cluster}} = 0.0126$ (M. F. Struble & H. J. Rood 1999), and a virial radius $R_{200} \sim 1.44 \pm 0.08$ Mpc (T. H. Reiprich & H. Bohringer 2002). Considering that Hydra I is at a distance of 59 Mpc (I. Jorgensen et al. 1996), we calculated the angular virial radius projecting R_{200} on the sky at 59 Mpc, giving $R_{200} \sim 1.4$ deg. The value of $5R_{200}$ is 7.2 Mpc (7 deg). All magnitudes are in the AB system (J. B. Oke & J. E. Gunn 1983).

5.1. Data

We used the catalogs from the 5th data release of S-PLUS (Lima et al., 2026, in preparation) to select a sample of galaxy candidates for H α emission, including the main photometric catalog and the Value Added Catalogs (VACs) of photometric redshift (photo-z) determinations (E. Lima et al. 2022) and galaxy-star-quasar classifications (L. Nakazono et al. 2021). The sample was cross-matched with the southern hemisphere redshift compilation (E. V. Lima 2025) to include the spectroscopic redshift for those objects that have it. To inspect the selected objects, we used images from S-PLUS and LS, as well as photometric and spectroscopic SEDs from S-PLUS and SDSS, respectively.

5.2. Method

First, we select a sample of S-PLUS objects by making a cone centered at the central position of Hydra I with a radius equals to $5R_{200}$ and applying the following constraints:

- $r_{\text{auto}} < 21$
- $0.001 < z_{\text{ml}} < 0.0326$
- $\text{PROB_GAL} \geq p$

r_{auto} is the r -band magnitude with auto aperture, z_{ml} is the photo-z, and PROB_GAL is the probability to be a galaxy.

We considered 0.02 as the maximum difference between the Hydra I cluster’s mean spectroscopic redshift and the object’s photo-z (z_{ml}) that an object can be considered a candidate for cluster membership. We also imposed the minimum value of 0.001 to the photo-z range because we noted, through visual inspection, that all objects with photo-z below this value are stars.

The probability threshold p varies depending on the galaxy’s r -band magnitude. Specifically, it is set to: 0.90 for magnitudes brighter than 16; 0.64 for magnitudes between 16 and 17; 0.92 for 17 to 18; 0.72 for 18 to 19; 0.58 for 19 to 20; and 0.30 for magnitudes fainter than 20.

Applying these constraints resulted in a sample containing 3,787 objects. We inspected the $F660 - (r + i)/2$ vs $F660$ color-magnitude diagram for this sample and made the following cut:

- $10 < F660_{\text{auto}} < 17$
- $-5 < F660_{\text{auto}} - (r_{\text{auto}} + i_{\text{auto}}) / 2 < 5$

That resulted in a subsample of 981 objects which we, finally, inspected using AstroInspect. $F660_{\text{auto}}$ and



Figure 5. Screenshot of the AstroInspect interface that allows mapping each of the 12 filters of the S-PLUS photometric system (u , F378, F395, F410, F430, g , F515, r , F660, i , F861, z) to a channel in the RGB (red, green, and blue) color space. The configuration shows the use of filters u , F378, F395, F410, F430, and g in the blue channel, F660 ($H\alpha$) alone in the green channel, and F515, r , i , F861, and z in the red channel. The flexibility of this visualization tool allows users to create color composites that determine how physical information will be visually encoded in the image.

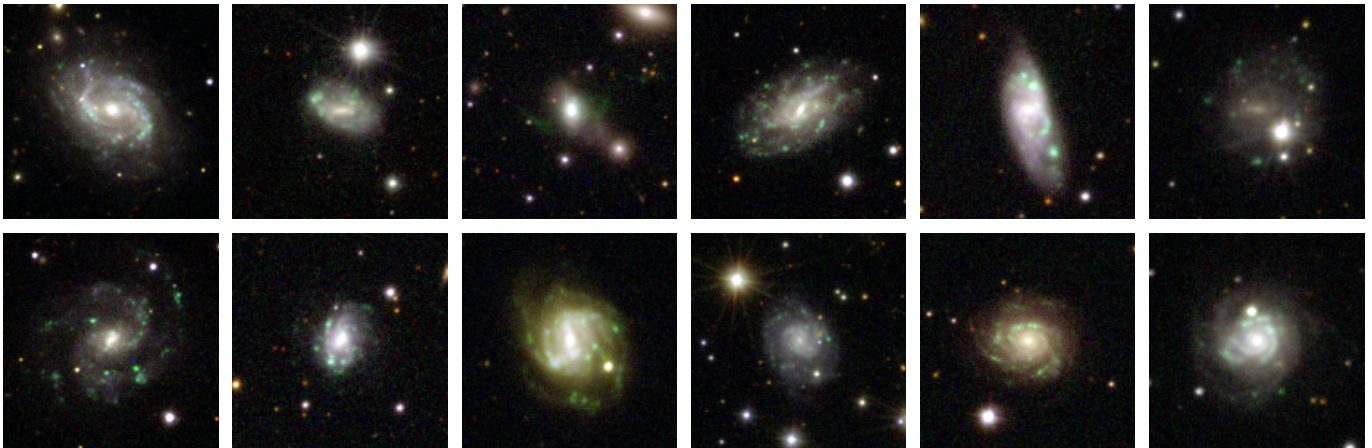


Figure 6. Mosaic of 12 $H\alpha$ emission galaxies in the direction of the Hydra I cluster found by visual inspection using AstroInspect. The images were created from the configuration indicated in Fig. 5, where only the F660 filter ($H\alpha$) was mapped to the green channel of the RGB image. This visualization setup enables a rapid identification of $H\alpha$ emission regions.

i_{auto} are the F660 and i -band magnitude with auto aperture, respectively.

We configured the stamp production through the AstroInspect interface to highlight $H\alpha$ -emission regions by mapping only the F660 filter to the green channel of the RGB image, as shown in Fig. 5. This allows for a quick identification of regions of interest during visual inspection.

5.3. Results

The visual inspection of candidate galaxies yielded a final sample of 80 $H\alpha$ emission-line galaxies in the direction of the Hydra I within the whole circle of radius $5R_{200}$. Of these, 63 have spec- z derived from E. V. Lima 2025, while the remaining 17 contains only photo- z derived from S-PLUS. Both the spec- z and photo- z measurements differ from z_{cluster} by no more than 0.02, supporting their association with the Hydra I cluster environment. A subset of these galaxies is presented in the mosaic in Fig. 6, and the complete catalog is available in Table 1. These results provide resources for future studies.

6. DISCUSSION

6.1. Case study analysis

$H\alpha$ emission is a key tracer of star-forming regions, as it originates from recombination in HII regions ionized by young, massive OB-type stars. Its presence indicates the existence of ionized gas and ongoing or star formation activity within galaxies. The high sensitivity of the S-PLUS F660 narrow-band filter enables the detection of $H\alpha$ emission from both extended star-forming regions in galactic disks and compact nuclear sources, making it a powerful tool for probing the spatial distribution and intensity of star formation across different galactic environments.

Visual selection of emission-line galaxies was essential to ensure the accurate identification of systems exhibiting significant $H\alpha$ emission, particularly given the morphological diversity and varying surface brightness of these features. As shown in Fig. 6, the $H\alpha$ emission exhibits a wide range of morphologies, from patchy, clumpy structures in spiral arms and irregular galaxies to more centrally concentrated emission in galactic nu-

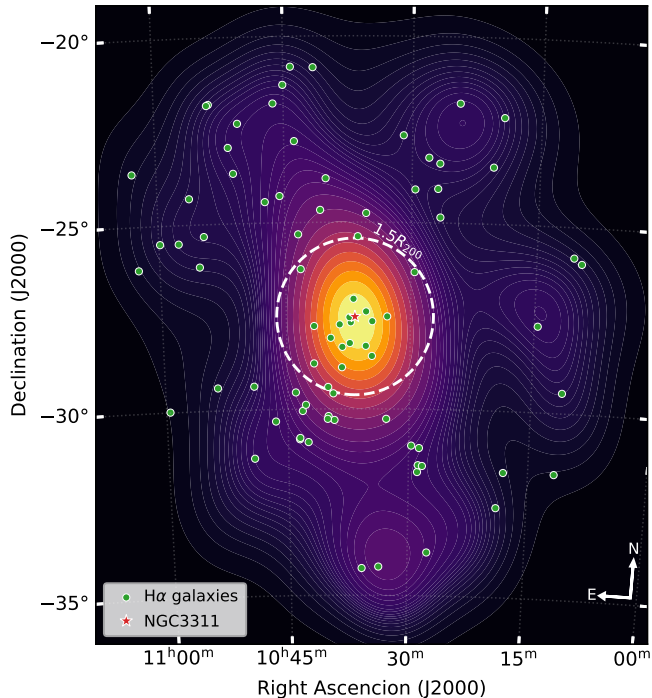


Figure 7. Comparison of the sample of 80 galaxies exhibiting H α emission (green dots) with the galaxy density in the Hydra I region. For the density visualization in the background, only galaxies with photo-z or spec-z between 0.001 and 0.0326 within a clustercentric distance of $5R_{200}$ were included. The dashed white circle delimits the $1.5R_{200}$ radius, and the red star indicates the position of the NGC3311, the Hydra’s brightest cluster galaxy (BCG).

clei. This diversity likely reflects different stages of star formation, feedback processes, and evolutionary histories, as well as variations in galaxy mass and morphology. The observed patterns highlight the importance of visual inspection in complementing automated methods, allowing a more nuanced assessment of the physical conditions and evolutionary states of star-forming galaxies.

Fig. 7 shows the spatial distribution of H α -emitting galaxies, identified through visual inspection, overlaid on the density of galaxies in the Hydra I region. The density map shown in the background considers only galaxies with redshift (spectroscopic, or photometric for those objects without known spectroscopy) in the range between 0.001 and 0.0326, and at a maximum distance of $5R_{200}$ from the cluster center.

Within $1.5R_{200}$, H α emitters are preferentially concentrated toward the southeast, while beyond this radius their distribution remains non-uniform. The resulting catalog provides a basis for future investigations of potential H α -emitting substructures in Hydra I using complementary data.

We noted that highlighting the H α component of galaxies directly in the AstroInspect interface greatly simplifies the identification of emission-line galaxies, enabling straightforward visual inspection.

Finally, we emphasize that this case study exemplifies the effectiveness of the AstroInspect in supporting visual inspection tasks, specially in galaxy morphology research. Its integrated interface enables a comprehensive galaxy characterization, combining imaging with photometric and spectroscopic information. For a more detailed discussion of the Hydra I cluster, we refer the reader to the literature. C. Lima-Dias et al. (2020, 2023) investigate the physical and structural properties of Hydra I, including analyses of H α -emitting galaxies. The forthcoming S-PLUS Clusters/Groups And their Large-scale Environments (SCALE; Mendes de Oliveira et al. 2026, in preparation) project will provide a comprehensive characterization of dozens of galaxy systems in the southern sky using combined spectroscopic and S-PLUS 12-band photometric data. With respect to Hydra I, this effort includes a detailed analysis of its dynamical properties (A. Ribeiro et al., in preparation) and a broader investigation of the large-scale environment of the Hydra–Antlia supercluster (A. Smith-Castelli et al., in preparation).

6.2. Benefits and trade-offs

Implementing AstroInspect as a web application has a direct impact on the user experience. The tool requires no compilation or installation, thereby enhancing accessibility. Its only prerequisite is a web browser, making it independent of operating systems and pre-installed system libraries. However, this design choice also constrains AstroInspect’s functionality to the web technologies supported by browsers, as standardized by the World Wide Web Consortium (W3C).

Cross-Origin Resource Sharing (CORS) is a W3C specification that defines a browser-enforced security mechanism for controlling cross-origin HTTP requests. Under this model, a web service must explicitly allow its resources to be accessed by applications originating from other domains. Otherwise, the browser blocks the request, even though the same resources may be accessible to desktop applications or standalone scripts. As a result, AstroInspect can interact only with external services that explicitly permit cross-origin access. This limitation was considered during system design, but a web-based implementation was adopted to prioritize accessibility, portability, and ease of use. A technical description of the CORS mechanism is provided in Appendix B.

Another limitation inherent to the use of web technologies is the limited access to the user’s file system, which directly affects the implementation of performance-enhancing mechanisms such as long-term caching. Nevertheless, emerging web API specifications, such as the File System Access API²⁷, may help mitigate this constraint once they achieve a broader adoption across browsers.

6.3. Comparison with other tools

TOPCAT is a well-established tool in astronomical research, providing robust functionalities for performing complex catalog operations. Despite its versatility, the visualization of image stamps in TOPCAT is limited to one object at a time, requiring repeated user input and reducing efficiency in tasks involving large samples.

Zooniverse²⁸ is a widely used platform for visual inspection in astronomy, with projects such as Galaxy Zoo (C. J. Lintott et al. 2008; C. Lintott et al. 2011) serving as notable examples. Its classification strategy is based on crowdsourcing, where contributions from many users are aggregated to produce reliable results. This approach has proven highly effective for large-scale citizen science initiatives (L. Hai-Ying et al. 2021; F. Didone et al. 2021).

In contrast to TOPCAT and Zooniverse, AstroInspect integrates catalog data and information from external services within a unified interface, streamlining the inspection process. This approach allows for use cases not directly supported by those tools, such as the quick classification of objects in catalogs by a single user.

6.4. Limitations

Tests conducted on various tables indicate that AstroInspect experiences performance degradation when handling tables exceeding 10 million cells. Additionally, AstroInspect relies on external services described in Section 2 and the unavailability of these services will directly impact the content displayed within the application.

7. CONCLUSION AND FUTURE WORK

Research groups working on galaxy morphology, particularly those relying on visual inspection, often require custom tools tailored to their specific workflows. AstroInspect was initially developed to support internal studies within our group, and after being successfully employed in multiple projects, it has now matured into

a general-purpose platform that can benefit the broader astronomical community.

In this work, we presented the first public release of the AstroInspect, a web-based system designed to streamline the visual inspection and scientific analysis of astronomical sources by integrating heterogeneous data products, such as images, spectra, and photometry, into a unified environment. Automated data retrieval, multi-survey integration, and configurable visualization options enhance efficiency in use cases such as morphological classification, catalog refinement, and exploratory analysis.

AstroInspect employs Pyodide, a WebAssembly-based Python runtime, to execute the scientific Python ecosystem directly in the browser. This client-side approach, increasingly adopted in scientific applications, provides access to widely used astronomical Python libraries without local installation or dedicated backend infrastructure. The system design presented in this work is adaptable to a range of use cases; for example, in data-intensive time-domain surveys such as the Vera C. Rubin Observatory’s Legacy Survey of Space and Time (LSST; Z. Ivezić et al. 2019), it can support the development of new applications designed for rapid visual inspection, preliminary characterization, and follow-up prioritization of transient events.

We exemplified the scientific value of AstroInspect through a case study targeting H α emission-line galaxies in the direction of the Hydra I cluster. Beginning with a photometric catalog of 981 S-PLUS candidates, the AstroInspect’s multi-band visualization and filtering capabilities enabled the rapid identification of 80 confirmed emission-line galaxies. This exercise highlights the effectiveness of the AstroInspect in supporting visual inspection tasks and provides a useful sample for studies of environmental effects in the Hydra I cluster.

Looking ahead, AstroInspect’s modular architecture supports straightforward integration with data from next-generation facilities. Upcoming wide-field spectroscopic surveys, such as the William Herschel Telescope Enhanced Area Velocity Explorer (WEAVE; S. Jin et al. 2024), the 4-metre Multi-Object Spectroscopic Telescope (4MOST; R. S. de Jong et al. 2012), and the Multi-Object Optical and Near-IR Spectrograph (MOONS; W. D. Taylor et al. 2018), will deliver extensive spectral datasets that can be directly incorporated to enhance visual inspection and analysis workflows.

DATA AVAILABILITY

The catalog of H α emission-line galaxies in the direction of the Hydra I cluster, described in Section 5, is available in the online version of this paper and the

²⁷ <https://wicg.github.io/file-system-access>

²⁸ <https://zooniverse.org>

columns description are shown in Table 1. We also provide a digital version of the catalog in various formats on our page²⁹.

ACKNOWLEDGMENTS

The S-PLUS project, including the T80-South robotic telescope and the S-PLUS scientific survey, was founded as a partnership between the Fundação de Amparo à Pesquisa do Estado de São Paulo (FAPESP), the Observatório Nacional (ON), the Federal University of Sergipe (UFS), and the Federal University of Santa Catarina (UFSC), with important financial and practical contributions from other collaborating institutes in Brazil, Chile (Universidad de La Serena), and Spain (Centro de Estudios de Física del Cosmos de Aragón, CEFCA). We further acknowledge financial support from the São Paulo Research Foundation (FAPESP), the Brazilian National Research Council (CNPq), the Coordination for the Improvement of Higher Education Personnel (CAPES), the Carlos Chagas Filho Rio de Janeiro State Research Foundation (FAPERJ), and the Brazilian Innovation Agency (FINEP).

The S-PLUS collaboration members are grateful for the contributions from CTIO staff in helping in the construction, commissioning, and maintenance of the T80-South telescope and camera. We are also indebted to Rene Laporte, INPE, and Keith Taylor for their essential contributions to the project. From CEFCA, we particularly would like to thank Antonio Marín-Franch for his invaluable contributions in the early phases of the project, David Cristóbal-Hornillos and his team for their help with the installation of the data reduction package JYPE version 0.9.9, César Íñiguez for providing 2D measurements of the filter transmissions, and all other staff members for their support with various aspects of the project.

Funding for the Sloan Digital Sky Survey V has been provided by the Alfred P. Sloan Foundation, the Heising-Simons Foundation, the National Science Foundation, and the Participating Institutions. SDSS acknowledges support and resources from the Center for High-Performance Computing at the University of Utah. SDSS telescopes are located at Apache Point Observatory, funded by the Astrophysical Research Consortium and operated by New Mexico State University, and at Las Campanas Observatory, operated by the Carnegie Institution for Science.

The Legacy Surveys consist of three individual and complementary projects: the Dark Energy Camera Legacy Survey (DECaLS; Proposal ID #2014B-0404; PIs: David Schlegel and Arjun Dey), the Beijing-Arizona Sky Survey (BASS; NOAO Prop. ID #2015A-0801; PIs: Zhou Xu and Xiaohui Fan), and the Mayall z-band Legacy Survey (MzLS; Prop. ID #2016A-0453; PI: Arjun Dey). DECaLS, BASS and MzLS together include data obtained, respectively, at the Blanco telescope, Cerro Tololo Inter-American Observatory, NSF’s NOIRLab; the Bok telescope, Steward Observatory, University of Arizona; and the Mayall telescope, Kitt Peak National Observatory, NOIRLab. Pipeline processing and analyses of the data were supported by NOIRLab and the Lawrence Berkeley National Laboratory (LBNL). The Legacy Surveys project is honored to be permitted to conduct astronomical research on Iolkam Du’ag (Kitt Peak), a mountain with particular significance to the Tohono O’odham Nation.

DESI construction and operations is managed by the Lawrence Berkeley National Laboratory. This research is supported by the U.S. Department of Energy, Office of Science, Office of High-Energy Physics, under Contract No. DE-AC02-05CH11231, and by the National Energy Research Scientific Computing Center, a DOE Office of Science User Facility under the same contract. Additional support for DESI is provided by the U.S. National Science Foundation, Division of Astronomical Sciences under Contract No. AST-0950945 to the NSF’s National Optical-Infrared Astronomy Research Laboratory; the Science and Technology Facilities Council of the United Kingdom; the Gordon and Betty Moore Foundation; the Heising-Simons Foundation; the French Alternative Energies and Atomic Energy Commission (CEA); the National Council of Science and Technology of Mexico (CONACYT); the Ministry of Science and Innovation of Spain, and by the DESI Member Institutions. The DESI collaboration is honored to be permitted to conduct astronomical research on Iolkam Du’ag (Kitt Peak), a mountain with particular significance to the Tohono O’odham Nation.

Guoshoujing Telescope (the Large Sky Area Multi-Object Fiber Spectroscopic Telescope LAMOST) is a National Major Scientific Project built by the Chinese Academy of Sciences. Funding for the project has been provided by the National Development and Reform Commission. LAMOST is operated and managed by the National Astronomical Observatories, Chinese Academy of Sciences.

This research has made use of the hips2fits, a tool developed at CDS, Strasbourg, France aiming at extract-

²⁹ <https://astroinspect.github.io/publications/hydra-halpha>

ing FITS images from HiPS sky maps with respect to a WCS.

This research uses services or data provided by the SPectra Analysis and Retrieval Catalog Lab (SPARCL) and the Astro Data Lab, which are both part of the Community Science and Data Center (CSDC) program at NSF National Optical-Infrared Astronomy Research Laboratory. NOIRLab is operated by the Association of Universities for Research in Astronomy (AURA), Inc. under a cooperative agreement with the National Science Foundation.

N.M.C. thanks the Coordenação de Aperfeiçoamento de Pessoal de Nível Superior – Brasil (CAPES) – Fi-

nance Code 88887.133104/2025-00. C.M.d.O. thanks Pesquisa do Estado de São Paulo (FAPESP) for funding through grants 2019/26492-3 and 2023/05087-9 and Conselho Nacional de Desenvolvimento Científico e Tecnológico (CNPq) through grant 309209/2019-6. A.C.K. thanks FAPESP for the support grant 2024/05467-9 and the CNPq. A.V.S.C. thanks financial support from Consejo Nacional de Investigaciones Científicas y Técnicas (CONICET) (PIP 1504), Agencia I+D+i (PICT 2019–03299) and Universidad Nacional de La Plata (Argentina). M.S.C acknowledges funding from FAPESP grant 2025/12629-8. R.D. thanks support by the ANID BASAL project FB210003.

APPENDIX

A. THE EMISSION-LINE CATALOG

We release a catalog of 80 $H\alpha$ emission-line galaxies in the direction of the Hydra I cluster, selected according to the procedure described in Section 5. The catalog includes multiwavelength photometry from S-PLUS DR5 and LS DR10, as well as spectroscopic redshifts when available. A description of the catalog columns is provided in Table 1.

Table 1. Column descriptions of the catalog containing the $H\alpha$ emission-line galaxies in the direction of the Hydra I cluster selected through visual inspection

#	Unit	Column name	Description
1		id	Catalog unique identifier
2	deg	ra	Right Ascension in decimal degrees (J2000)
3	deg	dec	Declination in decimal degrees (J2000)
4	mag	sp_mag_u	S-PLUS DR5 magnitude in the u band
5	mag	sp_mag_g	S-PLUS DR5 magnitude in the g band
6	mag	sp_mag_r	S-PLUS DR5 magnitude in the r band
7	mag	sp_mag_i	S-PLUS DR5 magnitude in the i band
8	mag	sp_mag_z	S-PLUS DR5 magnitude in the z band
9	mag	sp_mag_F378	S-PLUS DR5 magnitude in the F378 band (Balmer jump / [OII])
10	mag	sp_mag_F395	S-PLUS DR5 magnitude in the F395 band (Ca H + K)
11	mag	sp_mag_F410	S-PLUS DR5 magnitude in the F410 band ($H\delta$)
12	mag	sp_mag_F430	S-PLUS DR5 magnitude in the F430 band (G band)
13	mag	sp_mag_F515	S-PLUS DR5 magnitude in the F515 band (Mg b triplet)
14	mag	sp_mag_F660	S-PLUS DR5 magnitude in the F660 band ($H\alpha$)
15	mag	sp_mag_F861	S-PLUS DR5 magnitude in the F861 band (Ca triplet)
16–27	mag	sp_mag_err_ [band]	S-PLUS DR5 magnitude error, where [band] is one of: $u, g, r, i, z, F378, F395, F410, F430, F515, F660, F861$
28	deg	sp_A	S-PLUS DR5 profile RMS along the major axis
29	deg	sp_B	S-PLUS DR5 profile RMS along the minor axis

Table 1 *continued*

Table 1 (continued)

#	Unit	Column name	Description
30	deg	sp_PA	S-PLUS DR5 position angle (CCW/World-x)
31	deg	sp_radius_petro	S-PLUS DR5 petrosian apertures
32	deg	sp_radius_50	S-PLUS DR5 radius enclosing 50% of the total flux
33	deg	sp_radius_90	S-PLUS DR5 radius enclosing 90% of the total flux
34		sp_photoz	S-PLUS DR5 photometric redshift
35		sp_photoz_odds	S-PLUS DR5 photometric redshift odds
36	mag	ls_mag_g	LS DR10 magnitude in the <i>g</i> band
37	mag	ls_mag_r	LS DR10 magnitude in the <i>r</i> band
38	mag	ls_mag_i	LS DR10 magnitude in the <i>i</i> band
39	mag	ls_mag_z	LS DR10 magnitude in the <i>z</i> band
40		ls_type	LS DR10 morphological type (for details, see https://www.legacysurvey.org/dr10/description)
41		lit_redshift	Spectroscopic redshift
42		lit_redshift_err	Spectroscopic redshift error
43		lit_source	Spectroscopic redshift source from literature
44	km/s	velocity	Velocity derived from spectroscopic redshift
45	km/s	velocity_err	Velocity error
46	km/s	velocity_offset	Velocity difference between the object and the Hydra I, only available for objects with known spectroscopic redshift
47	deg	dist_proj	Sky projected angular distance between the object and the Hydra I cluster center
48	Mpc	dist	Distance between the object and the Hydra I cluster center, only available for objects with known spectroscopic redshift

NOTE—Columns prefixed with **sp** are drawn from S-PLUS DR5 (E. V. Lima et al. 2026, in preparation), while those prefixed with **ls** originate from Legacy Survey DR10 (A. Dey et al. 2019). Columns prefixed with **lit** originate from redshift compilation from the literature (E. V. Lima 2025). Columns without these prefixes were derived in this work. All magnitudes are reported in the AB system, and the S-PLUS magnitudes included in the catalog are only the auto-aperture values. This table is published in its entirety in the electronic edition of the *Astronomical Journal*. The columns description is shown here for guidance regarding its form and content.

B. TECHNICAL DESCRIPTION OF THE CROSS-ORIGIN RESOURCE SHARING

Cross-Origin Resource Sharing (CORS) is a browser-enforced security model configured through server-side HTTP response headers. For cross-origin requests, the browser determines whether a web application may access the response based solely on these headers. If the server does not explicitly authorize the requesting origin, the browser blocks the response from the application, even if the server successfully processed the request.

To illustrate the CORS mechanism in practice, we analyze a real HTTP response from the SkyServer (A. S. Szalay et al. 2002; M. Taghizadeh-Popp et al. 2020) service. Listing 1 presents the complete set of response headers returned by an HTTP request to SkyServer. The CORS-related headers appear in lines 10 to 12 of Listing 1.

The `Access-Control-Allow-Origin` header specifies which origins are permitted to access the response from a web application. In this example, its value is set to the wildcard character `*`, indicating that the resource is accessible from any origin. The browser interprets this as permission to expose the response to all client-side web applications, regardless of their domain. If this header were absent or restricted to a different origin, the browser would block access to the response.

The `Access-Control-Allow-Headers` header defines which custom request headers are allowed in cross-origin requests. Here, the value lists `Content-Type`, `X-Auth-Token`, and `Accept`, indicating that requests including these

headers are permitted. The `Access-Control-Allow-Methods` header specifies the HTTP methods (GET, POST, PUT, etc) allowed for cross-origin access. Its value is also set to `*`, meaning that all HTTP methods are accepted.

Together, these headers indicate that SkyServer explicitly allows cross-origin access without restrictions on origin or HTTP method. This example emphasizes that CORS does not constrain server-to-server communication. Instead, it governs how browsers expose cross-origin responses to client-side applications. Adopting permissive and well-defined CORS headers in astronomical web services is therefore a recommended best practice, as it enables browser-based scientific applications to access these services directly, broadening the ecosystem of web-enabled tools for astronomical data analysis.

```

1 HTTP/1.1 200 OK
2 cache-control: no-cache
3 pragma: no-cache
4 transfer-encoding: chunked
5 content-type: application/xml
6 expires: -1
7 server: Microsoft-IIS/10.0
8 x-aspnet-version: 4.0.30319
9 x-powered-by: ASP.NET
10 access-control-allow-origin: *
11 access-control-allow-headers: Content-Type, X-Auth-Token, Accept
12 access-control-allow-methods: *
13 date: Fri, 23 Jan 2026 11:59:22 GMT
14 strict-transport-security: max-age=63072000
15 content-security-policy: upgrade-insecure-requests
16 set-cookie: SERVERID=idieswww02; path=/

```

Listing 1. HTTP response headers returned by the SkyServer service, highlighting the CORS-related fields in lines 10 to 12 that permit access to its resources by web-based applications. To produce this example, we used the `cURL` command-line HTTP client with the following call: `curl -IX GET "https://skyserver.sdss.org/dr19/SkyServerWS/SpectroQuery/ConeSpectro?ra=344.5894&dec=-1.1839&radius=0.0833&limit=1&format=xml&specparams=specObjID"`

REFERENCES

- Abell, G. O., Corwin, Jr., H. G., & Olowin, R. P. 1989, *The Astrophysical Journal Supplement Series*, 70, 1, doi: [10.1086/191333](https://doi.org/10.1086/191333)
- Aihara, H., Armstrong, R., Bickerton, S., et al. 2018, *Publications of the Astronomical Society of Japan*, 70, S8, doi: [10.1093/pasj/psx081](https://doi.org/10.1093/pasj/psx081)
- Alexander, D. M., Davis, T. M., Chaussidon, E., et al. 2023, *The Astronomical Journal*, 165, 124, doi: [10.3847/1538-3881/acacfc](https://doi.org/10.3847/1538-3881/acacfc)
- Baillard, A., Bertin, E., De Lapparent, V., et al. 2011, *Astronomy & Astrophysics*, 532, A74, doi: [10.1051/0004-6361/201016423](https://doi.org/10.1051/0004-6361/201016423)
- Baumann, M., Boch, T., Pineau, F.-X., et al. 2020, in *Astronomical Data Analysis Software and Systems XXX. ASP Conference Series*, Vol. 532, Proceedings of a virtual conference held 8-12 November 2020., Vol. 532, *Astronomical Data Analysis Software and Systems XXX. ASP Conference Series*, ed. J. E. Ruiz, F. Pierfederici, & P. Teuben, virtual conference, Spain, 7, <https://hal.science/hal-03842974>
- Blum, R. D., Burleigh, K., Dey, A., et al. 2016, in *American Astronomical Society Meeting Abstracts #228*, Vol. 228, 317.01, <https://ui.adsabs.harvard.edu/abs/2016AAS...22831701B>
- Boch, T., Fitzpatrick, M., Taylor, M., et al. 2012, *Simple Application Messaging Protocol Version 1.3*, IVOA Recommendation 11 April 2012, doi: [10.5479/ADS/bib/2012ivoa.spec.0411B](https://doi.org/10.5479/ADS/bib/2012ivoa.spec.0411B)
- Boch, T., Oberto, A., Fernique, P., & Bonnarel, F. 2011, in *Astronomical Society of the Pacific Conference Series*, Vol. 442, *Astronomical Data Analysis Software and Systems XX*, ed. I. N. Evans, A. Accomazzi, D. J. Mink, & A. H. Rots, 683
- Bom, C. R., Cortesi, A., Lucatelli, G., et al. 2021, *Monthly Notices of the Royal Astronomical Society*, 507, 1937–1955, doi: [10.1093/mnras/stab1981](https://doi.org/10.1093/mnras/stab1981)
- Bonnarel, F., Fernique, P., Bienaymé, O., et al. 2000, *Astronomy and Astrophysics, Supplement*, 143, 33, doi: [10.1051/aas:2000331](https://doi.org/10.1051/aas:2000331)

- Boyce, M. M., Hopkins, A. M., Riggi, S., et al. 2023, Publications of the Astronomical Society of Australia, 40, e028, doi: [10.1017/pasa.2023.24](https://doi.org/10.1017/pasa.2023.24)
- Busko, I. 2000, in Astronomical Society of the Pacific Conference Series, Vol. 216, Astronomical Data Analysis Software and Systems IX, 79.
<https://ui.adsabs.harvard.edu/abs/2000ASPC..216...79B>
- Busko, I. 2002, in Astronomical Society of the Pacific Conference Series, Vol. 281, Astronomical Data Analysis Software and Systems XI, 120.
<https://ui.adsabs.harvard.edu/abs/2002ASPC..281..120B>
- Cardoso, N. M., Schwarz, G. B., Dias, L. O., et al. 2021, Notas Técnicas, 11, 1–18,
doi: [10.7437/nt2236-7640/2021.02.002](https://doi.org/10.7437/nt2236-7640/2021.02.002)
- Chambers, K. C., Magnier, E. A., Metcalfe, N., et al. 2016, The Pan-STARRS1 Surveys, arXiv,
doi: [10.48550/arXiv.1612.05560](https://doi.org/10.48550/arXiv.1612.05560)
- Cui, X.-Q., Zhao, Y.-H., Chu, Y.-Q., et al. 2012, Research in Astronomy and Astrophysics, 12, 1197,
doi: [10.1088/1674-4527/12/9/003](https://doi.org/10.1088/1674-4527/12/9/003)
- Darg, D. W., Kaviraj, S., Lintott, C. J., et al. 2010, Monthly Notices of the Royal Astronomical Society, 401, 1552, doi: [10.1111/j.1365-2966.2009.15786.x](https://doi.org/10.1111/j.1365-2966.2009.15786.x)
- Dark Energy Survey Collaboration, Abbott, T., Abdalla, F. B., et al. 2016, Monthly Notices of the Royal Astronomical Society, 460, 1270,
doi: [10.1093/mnras/stw641](https://doi.org/10.1093/mnras/stw641)
- de Jong, R. S., Bellido-Tirado, O., Chiappini, C., et al. 2012, in Ground-based and Airborne Instrumentation for Astronomy IV, Vol. 8446, eprint: arXiv:1206.6885, 84460T, doi: [10.1117/12.926239](https://doi.org/10.1117/12.926239)
- DESI Collaboration, Aghamousa, A., Aguilar, J., et al. 2016, The DESI Experiment Part I: Science, Targeting, and Survey Design, arXiv,
doi: [10.48550/arXiv.1611.00036](https://doi.org/10.48550/arXiv.1611.00036)
- Dey, A., Schlegel, D. J., Lang, D., et al. 2019, The Astronomical Journal, 157, 168,
doi: [10.3847/1538-3881/ab089d](https://doi.org/10.3847/1538-3881/ab089d)
- Didone, F., Richter, A., Esra, P., Baiba, P., & Katrin, V. 2021, in The Science of Citizen Science, ed. V. Katrin, A. Land-Zandstra, C. Luigi, L. Rob, P. Josep, P. Marisa, S. Roeland, & W. Katherin (Cham: Springer International Publishing), 79–96,
doi: [10.1007/978-3-030-58278-4_5](https://doi.org/10.1007/978-3-030-58278-4_5)
- Dijkstra, E. W. 1968, in The Origin of Concurrent Programming, ed. P. B. Hansen (New York, NY: Springer New York), 65–138, doi: [10.1007/978-1-4757-3472-0_2](https://doi.org/10.1007/978-1-4757-3472-0_2)
- Dijkstra, E. W. 1972, Information Processing Letters, 1, 179, doi: [10.1016/0020-0190\(72\)90034-8](https://doi.org/10.1016/0020-0190(72)90034-8)
- Draper, P. W. 2014, Astrophysics Source Code Library, ascl:1402.007.
<https://ui.adsabs.harvard.edu/abs/2014ascl.soft02007D>
- Dye, S., Lawrence, A., Read, M. A., et al. 2018, Monthly Notices of the Royal Astronomical Society, 473, 5113,
doi: [10.1093/mnras/stx2622](https://doi.org/10.1093/mnras/stx2622)
- Epchtein, N., de Batz, B., Capoani, L., et al. 1997, The Messenger, 87, 27.
<https://ui.adsabs.harvard.edu/abs/1997Msngr..87...27E>
- Fernique, P., Allen, M. G., Boch, T., et al. 2015, Astronomy & Astrophysics, 578, A114,
doi: [10.1051/0004-6361/201526075](https://doi.org/10.1051/0004-6361/201526075)
- Fitzpatrick, M., Olsen, K., Eychaner, G., et al. 2019, in Astronomical Data Analysis Software and Systems XXVII, Vol. 523, 233.
<https://ui.adsabs.harvard.edu/abs/2019ASPC..523..233F>
- Fukugita, M., Ichikawa, T., Gunn, J. E., et al. 1996, The Astronomical Journal, 111, 1748, doi: [10.1086/117915](https://doi.org/10.1086/117915)
- Galdeano, D., Coldwell, G., Alonso, S., et al. 2025, Astronomy & Astrophysics, 698, A214,
doi: [10.1051/0004-6361/202554268](https://doi.org/10.1051/0004-6361/202554268)
- Gallagher, Iii, J. S., & Ostriker, J. P. 1972, The Astronomical Journal, 77, 288, doi: [10.1086/111280](https://doi.org/10.1086/111280)
- Gunn, J. E., & Gott, Iii, J. R. 1972, The Astrophysical Journal, 176, 1, doi: [10.1086/151605](https://doi.org/10.1086/151605)
- Gunn, J. E., Siegmund, W. A., Mannery, E. J., et al. 2006, The Astronomical Journal, 131, 2332–2359,
doi: [10.1086/500975](https://doi.org/10.1086/500975)
- Hai-Ying, L., Dörler, D., Florian, H., & Sonja, G. 2021, in The Science of Citizen Science, ed. V. Katrin, A. Land-Zandstra, C. Luigi, L. Rob, P. Josep, P. Marisa, S. Roeland, & W. Katherin (Cham: Springer International Publishing), 439–459,
doi: [10.1007/978-3-030-58278-4_22](https://doi.org/10.1007/978-3-030-58278-4_22)
- Harris, K. D., & Greenbaum, G. 2024, Nucleic Acids Research, 52, W54, doi: [10.1093/nar/gkae373](https://doi.org/10.1093/nar/gkae373)
- Heil, S., Schröder, L., & Gaedke, M. 2025, in Web Information Systems Engineering – WISE 2024, ed. M. Barhamgi, H. Wang, & X. Wang, Vol. 15440 (Singapore: Springer Nature Singapore), 500–511,
doi: [10.1007/978-981-96-0576-7_36](https://doi.org/10.1007/978-981-96-0576-7_36)
- Hunter, J. D. 2007, Matplotlib: A 2D Graphics Environment, Institute of Electrical and Electronics Engineers (IEEE), doi: [10.1109/mcse.2007.55](https://doi.org/10.1109/mcse.2007.55)
- Ivezić, Z., et al. 2019, The Astrophysical Journal, 873, 111,
doi: [10.3847/1538-4357/AB042C](https://doi.org/10.3847/1538-4357/AB042C)
- Jaffé, Y. L., Smith, R., Candlish, G. N., et al. 2015, Monthly Notices of the Royal Astronomical Society, 448, 1715, doi: [10.1093/mnras/stv100](https://doi.org/10.1093/mnras/stv100)

- Ji, D., Aboukhalil, R., & Moshiri, N. 2024, *Bioinformatics*, 40, btae018, doi: [10.1093/bioinformatics/btae018](https://doi.org/10.1093/bioinformatics/btae018)
- Jin, S., Trager, S. C., Dalton, G. B., et al. 2024, *Monthly Notices of the Royal Astronomical Society*, 530, 2688, doi: [10.1093/mnras/stad557](https://doi.org/10.1093/mnras/stad557)
- Jorgensen, I., Franx, M., & Kjaergaard, P. 1996, *Monthly Notices of the Royal Astronomical Society*, 280, 167, doi: [10.1093/mnras/280.1.167](https://doi.org/10.1093/mnras/280.1.167)
- Joye, W. A., & Mandel, E. 2003, in *Astronomical Society of the Pacific Conference Series*, Vol. 295, *Astronomical Data Analysis Software and Systems XII*, ed. H. E. Payne, R. I. Jedrzejewski, & R. N. Hook, 489
- Juneau, S., Jacques, A., Pothier, S., et al. 2024, SPARCL: SPectra Analysis and Retrievable Catalog Lab, arXiv, doi: [10.48550/ARXIV.2401.05576](https://doi.org/10.48550/ARXIV.2401.05576)
- Kartaltepe, J. S., Mozena, M., Kocevski, D., et al. 2015, *The Astrophysical Journal Supplement Series*, 221, 11, doi: [10.1088/0067-0049/221/1/11](https://doi.org/10.1088/0067-0049/221/1/11)
- Krabbe, A. C., Hernandez-Jimenez, J. A., Mendes de Oliveira, C., et al. 2023, *Monthly Notices of the Royal Astronomical Society*, 528, 1125–1141, doi: [10.1093/mnras/stad3881](https://doi.org/10.1093/mnras/stad3881)
- Lacy, M., Baum, S. A., Chandler, C. J., et al. 2020, *Publications of the Astronomical Society of the Pacific*, 132, 035001, doi: [10.1088/1538-3873/ab63eb](https://doi.org/10.1088/1538-3873/ab63eb)
- Lambas, D. G., Alonso, S., Mesa, V., & O'mill, A. L. 2012, *A&A*, 539, 45, doi: [10.1051/0004-6361/201117900](https://doi.org/10.1051/0004-6361/201117900)
- Lang, D. 2014, *The Astronomical Journal*, 147, 108, doi: [10.1088/0004-6256/147/5/108](https://doi.org/10.1088/0004-6256/147/5/108)
- Lawrence, A., Warren, S. J., Almaini, O., et al. 2007, *Monthly Notices of the Royal Astronomical Society*, 379, 1599, doi: [10.1111/j.1365-2966.2007.12040.x](https://doi.org/10.1111/j.1365-2966.2007.12040.x)
- Lima, E., Sodr e, L., Bom, C., et al. 2022, *Astronomy and Computing*, 38, 100510, doi: [10.1016/j.ascom.2021.100510](https://doi.org/10.1016/j.ascom.2021.100510)
- Lima, E. V. 2025, *Southern Hemisphere Spectroscopic Redshift Compilation*, Zenodo, doi: [10.5281/ZENODO.15127060](https://doi.org/10.5281/ZENODO.15127060)
- Lima-Dias, C., Monachesi, A., Torres-Flores, S., et al. 2020, *Monthly Notices of the Royal Astronomical Society*, 500, 1323, doi: [10.1093/mnras/staa3326](https://doi.org/10.1093/mnras/staa3326)
- Lima-Dias, C., Monachesi, A., Torres-Flores, S., et al. 2023, *Monthly Notices of the Royal Astronomical Society*, 527, 5792, doi: [10.1093/mnras/stad3571](https://doi.org/10.1093/mnras/stad3571)
- Lintott, C., Schawinski, K., Bamford, S., et al. 2011, *Monthly Notices of the Royal Astronomical Society*, 410, 166, doi: [10.1111/J.1365-2966.2010.17432.X](https://doi.org/10.1111/J.1365-2966.2010.17432.X)
- Lintott, C. J., Schawinski, K., Slosar, A., et al. 2008, *Monthly Notices of the Royal Astronomical Society*, 389, 1179, doi: [10.1111/J.1365-2966.2008.13689.X](https://doi.org/10.1111/J.1365-2966.2008.13689.X)
- Martin, D. C., Fanson, J., Schiminovich, D., et al. 2005, *The Astrophysical Journal*, 619, L1, doi: [10.1086/426387](https://doi.org/10.1086/426387)
- Matilsky, T. 2020, *Phys. Teach.*, 58, 602, doi: [10.1119/10.0002391](https://doi.org/10.1119/10.0002391)
- Mendes de Oliveira, C., Ribeiro, T., Schoenell, W., et al. 2019, *Monthly Notices of the Royal Astronomical Society*, 489, 241, doi: [10.1093/mnras/stz1985](https://doi.org/10.1093/mnras/stz1985)
- Moore, B., Katz, N., Lake, G., Dressler, A., & Oemler, A. 1996, *Nature*, 379, 613, doi: [10.1038/379613a0](https://doi.org/10.1038/379613a0)
- Nair, P. B., & Abraham, R. G. 2010, *Astrophysical Journal Supplement Series*, 186, 427, doi: [10.1088/0067-0049/186/2/427](https://doi.org/10.1088/0067-0049/186/2/427)
- Nakazono, L., Mendes de Oliveira, C., Hirata, N. S. T., et al. 2021, *Monthly Notices of the Royal Astronomical Society*, 507, 5847, doi: [10.1093/mnras/stab1835](https://doi.org/10.1093/mnras/stab1835)
- Nikutta, R., Fitzpatrick, M., Scott, A., & Weaver, B. 2020, *Astronomy and Computing*, 33, 100411, doi: [10.1016/j.ascom.2020.100411](https://doi.org/10.1016/j.ascom.2020.100411)
- Oke, J. B., & Gunn, J. E. 1983, *The Astrophysical Journal*, 266, 713, doi: [10.1086/160817](https://doi.org/10.1086/160817)
- Onken, C. A., Wolf, C., Bessell, M. S., et al. 2024, *Publications of the Astronomical Society of Australia*, 41, e061, doi: [10.1017/pasa.2024.53](https://doi.org/10.1017/pasa.2024.53)
- Paillou, P., Bonnarel, F., Ochsenbein, F., & Cr ez e, M. 1994, *Symposium - International Astronomical Union*, 161, 347, doi: [10.1017/S0074180900047628](https://doi.org/10.1017/S0074180900047628)
- Panagoulia, E. K., Fabian, A. C., & Sanders, J. S. 2014, *Monthly Notices of the Royal Astronomical Society*, 438, 2341, doi: [10.1093/mnras/stt2349](https://doi.org/10.1093/mnras/stt2349)
- Paudel, S., Smith, R., Yoon, S. J., Calder on-Castillo, P., & Duc, P.-A. 2018, *The Astrophysical Journal Supplement Series*, 237, 36, doi: [10.3847/1538-4365/AAD555](https://doi.org/10.3847/1538-4365/AAD555)
- Peeters, R., Rodriguez Martin, L., Zhang, F., et al. 2025, *International Journal of Hygiene and Environmental Health*, 270, 114669, doi: [10.1016/j.ijheh.2025.114669](https://doi.org/10.1016/j.ijheh.2025.114669)
- Plante, R., Williams, R., Hanisch, R., & Szalay, A. 2008, *Simple Cone Search Version 1.03*, IVOA Recommendation 22 February 2008, doi: [10.5479/ADS/bib/2008ivoa.specQ0222P](https://doi.org/10.5479/ADS/bib/2008ivoa.specQ0222P)
- Reiprich, T. H., & Bohringer, H. 2002, *The Astrophysical Journal*, 567, 716, doi: [10.1086/338753](https://doi.org/10.1086/338753)
- Šaloun, P., Andrešič, D., Škoda, P., & Zelinka, I. 2016, in *2016 International Conference on Systems Informatics, Modelling and Simulation (SIMS)*, Riga, Latvia, 111–116, doi: [10.1109/SIMS.2016.20](https://doi.org/10.1109/SIMS.2016.20)
- Schwarz, G. O., Herpich, F., Almeida-Fernandes, F., et al. 2025, *Astronomy and Computing*, 51, 100899, doi: [10.1016/j.ascom.2024.100899](https://doi.org/10.1016/j.ascom.2024.100899)

- Silva, D. R., Blum, R. D., Allen, L., et al. 2016, in American Astronomical Society Meeting Abstracts #228, Vol. 228, 317.02.
<https://ui.adsabs.harvard.edu/abs/2016AAS...22831702S>
- Škoda, P., Draper, P. W., Neves, M. C., Andrešič, D., & Jenness, T. 2014, *Astronomy and Computing*, 7–8, 108, doi: [10.1016/j.ascom.2014.06.001](https://doi.org/10.1016/j.ascom.2014.06.001)
- Skrutskie, M. F., Cutri, R. M., Stiening, R., et al. 2006, *The Astronomical Journal*, 131, 1163, doi: [10.1086/498708](https://doi.org/10.1086/498708)
- Smee, S. A., Gunn, J. E., Uomoto, A., et al. 2013, *The Astronomical Journal*, 146, 32, doi: [10.1088/0004-6256/146/2/32](https://doi.org/10.1088/0004-6256/146/2/32)
- Smith Castelli, A. V., Cortesi, A., Haack, R. F., et al. 2024, *Monthly Notices of the Royal Astronomical Society*, 530, 3787–3811, doi: [10.1093/mnras/stae840](https://doi.org/10.1093/mnras/stae840)
- Struble, M. F., & Rood, H. J. 1999, *The Astrophysical Journal Supplement Series*, 125, 35, doi: [10.1086/313274](https://doi.org/10.1086/313274)
- Szalay, A. S., Gray, J., Thakar, A. R., et al. 2002, in *Proceedings of the 2002 ACM SIGMOD International Conference on Management of Data, SIGMOD '02* (New York, NY, USA: Association for Computing Machinery), 570–581, doi: [10.1145/564691.564758](https://doi.org/10.1145/564691.564758)
- Taghizadeh-Popp, M., Kim, J., Lemson, G., et al. 2020, *Astronomy and Computing*, 33, 100412, doi: <https://doi.org/10.1016/j.ascom.2020.100412>
- Tan, L., Mei, Y., Qian, J., et al. 2025, *The Astrophysical Journal Supplement Series*, 280, 24, doi: [10.3847/1538-4365/adf4e6](https://doi.org/10.3847/1538-4365/adf4e6)
- Taylor, M. 2017, *Informatics*, 4, doi: [10.3390/informatics4030018](https://doi.org/10.3390/informatics4030018)
- Taylor, M. B. 2005, *ASPC*, 347, 29. <https://ui.adsabs.harvard.edu/abs/2005ASPC..347...29T/abstract>
- Taylor, M. B. 2006, in *Astronomical Society of the Pacific Conference Series*, Vol. 351, *Astronomical Data Analysis Software and Systems XV*, San Lorenzo de El Escorial, Spain, 666.
<https://ui.adsabs.harvard.edu/abs/2006ASPC..351..666T>
- Taylor, M. B., Boch, T., & Taylor, J. 2015, *Astronomy and Computing*, 11, 81, doi: [10.1016/J.ASCOM.2014.12.007](https://doi.org/10.1016/J.ASCOM.2014.12.007)
- Taylor, W. D., Cirasuolo, M., Afonso, J., et al. 2018, in *Ground-based and Airborne Instrumentation for Astronomy VII*, ed. H. Takami, C. J. Evans, & L. Simard (Austin, United States: SPIE), 52, doi: [10.1117/12.2313403](https://doi.org/10.1117/12.2313403)
- The Astropy Collaboration, Robitaille, T. P., Tollerud, E. J., et al. 2013, *Astronomy & Astrophysics*, 558, A33, doi: [10.1051/0004-6361/201322068](https://doi.org/10.1051/0004-6361/201322068)
- The Astropy Collaboration, Price-Whelan, A. M., Sipőcz, B. M., et al. 2018, *The Astronomical Journal*, 156, 123, doi: [10.3847/1538-3881/aabc4f](https://doi.org/10.3847/1538-3881/aabc4f)
- The Astropy Collaboration, Price-Whelan, A. M., Lim, P. L., et al. 2022, *The Astrophysical Journal*, 935, 167, doi: [10.3847/1538-4357/ac7c74](https://doi.org/10.3847/1538-4357/ac7c74)
- Torrens-Fontanals, M., Turlas, P., Doerr, S., & De Fabritiis, G. 2024, *Journal of Chemical Information and Modeling*, 64, 584, doi: [10.1021/acs.jcim.3c01776](https://doi.org/10.1021/acs.jcim.3c01776)
- Warren, S. J., Hambly, N. C., Dye, S., et al. 2007, *Monthly Notices of the Royal Astronomical Society*, 375, 213, doi: [10.1111/j.1365-2966.2006.11284.x](https://doi.org/10.1111/j.1365-2966.2006.11284.x)
- Wright, E. L., Eisenhardt, P. R. M., Mainzer, A. K., et al. 2010, *The Astronomical Journal*, 140, 1868, doi: [10.1088/0004-6256/140/6/1868](https://doi.org/10.1088/0004-6256/140/6/1868)
- York, D., Adelman, J., Anderson, J., et al. 2000, *Astronomical Journal*, 120, 1579, doi: [10.1086/301513](https://doi.org/10.1086/301513)
- Zhao, G., Zhao, Y.-H., Chu, Y.-Q., Jing, Y.-P., & Deng, L.-C. 2012, *Research in Astronomy and Astrophysics*, 12, 723, doi: [10.1088/1674-4527/12/7/002](https://doi.org/10.1088/1674-4527/12/7/002)
- Zou, H., Zhou, X., Fan, X., et al. 2017, *Publications of the Astronomical Society of the Pacific*, 129, 064101, doi: [10.1088/1538-3873/aa65ba](https://doi.org/10.1088/1538-3873/aa65ba)
- Žáková, K., & Beňačka, C. 2025, *IFAC-PapersOnLine*, 59, 83, doi: [10.1016/j.ifacol.2025.08.027](https://doi.org/10.1016/j.ifacol.2025.08.027)